Journal of Japan Society of Civil Engineers, Ser.
A1 (Structural Engineering & Earthquake Engineering (SE/EE)), Vol. 68, No. 3, 526-541, 2012.

APPLICATION OF RHEOLOGY MODELING TO NATURAL RUBBER AND LEAD RUBBER BEARINGS: A SIMPLIFIED MODEL AND LOW TEMPERATURE BEHAVIOR

Muhammad Kashif RAZZAQ[1], Yoshiaki OKUI[2], Abdur Rahman BHUIYAN[3], A.F.M. Saiful AMIN[4], Hiroshi MITAMURA[5]and Takashi IMAI[6]

[1]Assistant Prof., Dept. of Civil Engi., National University of Computer & Emerging Sciences (FAST-NU) (Lahore 54700, Pakistan)
E-mail: muhdkashifrazzaq@gmail.com
[2]Member of JSCE, Prof., Dept. of Civil and Environmental Eng., Saitama University (255, Shimo-Okubo, Sakura, Saitama, 338-8570, Japan)
E-mail: okui@mail.saitama-u.ac.jp
[3]Assoc. Prof., Dept. of Civil Eng., Chittagong University of Engineering and Technology (Chittagong 4349, Bangladesh)
[4]Prof., Dept. of Civil Eng., Bangladesh University of Engineering and Technology (Dhaka 1000, Bangladesh)
[5]Civil Engineering Research Institute for Cold Region, PWRI (Hiragishi 1-3-1-34 Toyohira-ku, Sapporo 062-8602, Japan)
[6]Rubber Bearing Association (Tobu Building, Moto Akasaka 1-5-26, Minato-ku, Tokyo 107-0051, Japan)

A rheology originally proposed for high damping rubber bearing (HDRB) is applied to natural rubber bearing (RB) and lead rubber bearing (LRB) along with its simplified form. Comparing HDRB, the elastic-plastic equilibrium responses were found to be more dominant than the rate-dependent response due to viscosity for RB and LRB. Moreover, the overstress in loading/unloading was found to be analogous. The dependency of nonlinear viscosity on current strain was found to be weak in contrast to the existence of considerable nonlinearity in elastic response. The original rheology model considers the nonlinear elasto-plastic and viscosity induced rate-dependent behavior into account, while the viscosity effect is eliminated in the simplified version. The models are implemented in a finite element code. The modeling effects of bearings on the seismic responses of a multi-span continuous highway bridge are investigated via nonlinear dynamic analyses for two strong earthquake ground motions. Three analytical models of isolation bearings are considered for comparison: the conventional design models and the proposed two models. Model parameters for the bearings were determined for two temperature conditions: the room temperature (+23 °C) and the low temperature (-20°C) based on experimental data. The implication of the rheology models for response prediction of a prototype bridge is studied by comparing the rotation of a plastic hinge in pier and shear strain at the top of the bearing. The comparison suggests that the modeling of RB and LRB considering rheology properties is important for rational prediction of the seismic response of highway bridges, particularly at low temperature condition.

Key Words : *nonlinear dynamic analysis, seismic response, rheology model, bilinear model, damping, elasticity, rate-dependency*

1. INTRODUCTION

The use of rubber bearing in base isolation technique for seismic protection is much older than the development of high damping rubber bearings (HDRBs). The earlier attempt for base isolation depended mostly on the low stiffness of the natural rubber bearings (RBs) to attain the desired isolation effect. Insertion of lead plugs in rubber bearings (LRBs) provided additional hysteresis properties under cyclic loads[1)] to reduce responses against stronger earthquakes.

The dissertation[2)] and the earlier communications[3)] addressed the rationality of developing a model for HDRBs based on rheological characterization. The necessity to study the effect of such modeling on response prediction of a prototype bridge superstructure-pier-foundation (S-P-F) system due to severe earthquakes[4)] (Level 2; Type I and Type II) is also revealed through examples. As opposed to the

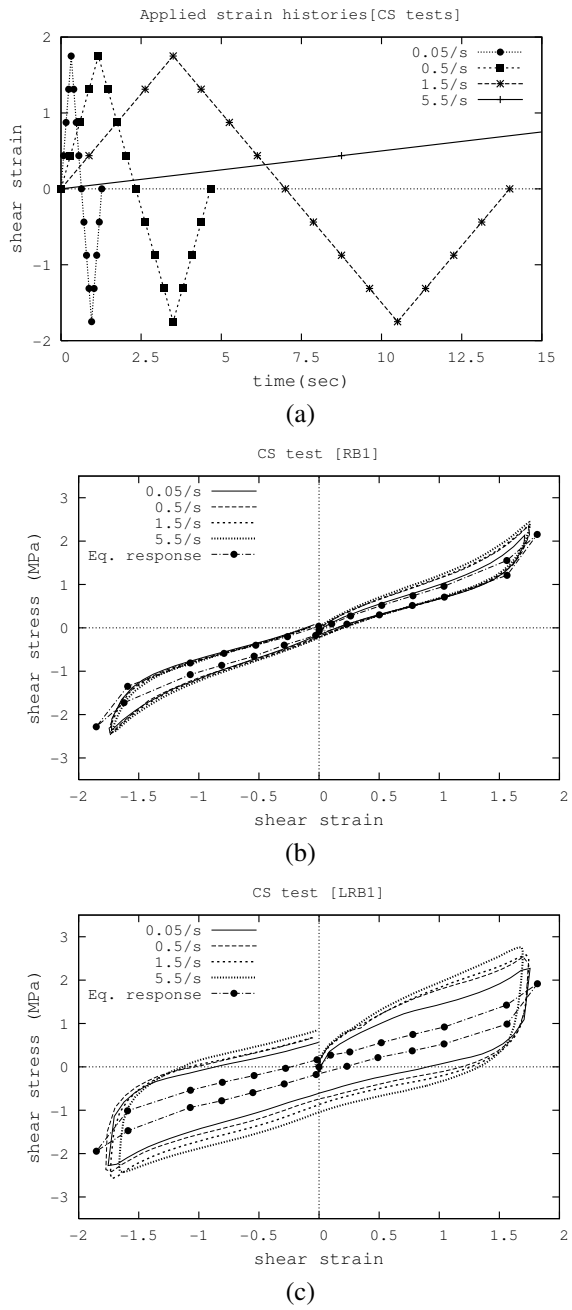

Fig.1 Shear stress-strain relationships obtained from the cyclic shear (CS) tests at different strain rates at room temperature. (a) Applied strain history, (b) RB, (c) LRB; equilibrium response obtained from MSR test data is also accompanied by the CS test data for comparison.

conventional design models[4),5),6)] that solely consider linear or bilinear rate-independent elasto-plastic properties of the rubber bearings, we have shown the existence of nonlinear elasticity, viscosity and plasticity effects in HDRBs through experiments[7),8)]. The current paper deals with developing models for RBs and LRBs through a systematic rheological characterization and presents the comparisons of modeling ef-

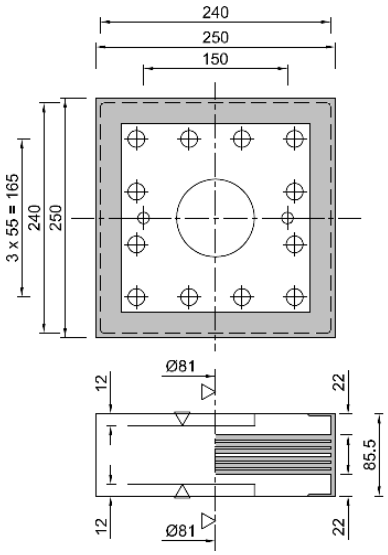

Fig.2 Specimen of laminated bearing; Bearing dimensions are presented in **Table 1**.

Table1 Geometric dimensions of RB and LRB.

Particulars	Specifications
Cross-section (mm^2)	240×240
Number of rubber layers	6
Thickness of one rubber layer (mm)	5
Thickness of steel layer (mm)	2.3
Nominal shear Modulus (MPa)	1.2
Number of lead plugs for LRB	4
Diameter of lead plug for LRB (mm)	34.5

fects on seismic response prediction of the prototype bridge.

Fig. 1 presents the typical responses from RB and LRB at different strain rates. **Fig. 1a** shows the applied strain histories, which are triangle waves with four different shear strain rates ranging from 0.05 to 5.5 /s. In this figure, only the first 15 seconds of the strain histories are shown, and accordingly the latter part of strain history for the slowest strain rate of 0.05 /s is truncated. **Fig. 1b, 1c** are obtained stress-strain curves for different strain rates; see dissertation[2)] for more details.

Both bearings are of the same geometry (**Fig. 2** and **Table 1**) and the same compound of rubber material. The only difference is the existence of four lead plugs in the LRB. Therefore, the difference in responses between the two bearings can only be attributed to the presence of lead plugs. In order to clarify the rate-independent plasticity effect in both bearings, the equilibrium response obtained from a Multi-Step Relaxation (MSR) test[3)] are plotted. By comparing the responses from RB and LRB, it is interesting to note that in LRB, both rate-dependency and plasticity ef-

fects are much pronounced than those in RB. In comparison to HDRB, the extents of all these effects are found to be much smaller[2),3)]. These observations motivate us for further examining the responses with a view to arrive at rational models for these two types of bearings. In addition, the recent contributions from Yakut and Yura[9),10)] and Amin *et al.*[11)] can be referred to, where information about the behavior of rubber at low temperature is presented. They report a marked increase in stiffness, nonlinearity in the stress-strain responses and rate-dependency property at low temperature. Hence, it is also important to verify the adequacy of the model parameters for RB and LRB not only at the room temperature but also at a low temperature.

In this paper, a rate-dependent rheology model and a simplified version of the rheology model eliminating the viscosity effect are presented for LRB and RB. The proposed models resulted from the modification of the rheology model[3)] originally proposed for HDRB. In the second part of the paper, the developed models have been used to generate the finite element model of a standard continuous span highway bridge, where nonlinear force-displacement relation of the pier and deformation of the foundation were also incorporated. In this process, the effect of modeling of bearings in the numerical analysis of the standard bridge S-P-F system is studied by conducting the nonlinear dynamic analysis of the system and comparing the responses in terms of shear strain of the bearings and rotation of the bridge pier. Three models of the bearings were employed for comparison: conventional design models and two rheology models under two temperature conditions.

2. MEASUREMENTS

Two specimen sets, referred to as RB, RB-2 and LRB, LRB-2 were used. The self-contained and typical experimental results obtained from RB and LRB specimens are presented in this paper briefly; however, results from other sets of specimens are available from the recent dissertation[2)]. The geometry and material properties of these specimens are given in **Table 1**.

The dimensions of the test specimens were selected in accordance with ISO standard[12)]. To eliminate the effects of past loading histories on the measured specimen response, tests were carried out every time on a new specimen. All specimens were tested under shear deformation with an average constant vertical compressive stress of 6 MPa. This mode of deformation is regarded as the most relevant one for application in seismic isolation[13)]. A computer-controlled servo hydraulic testing machine was used, and the displacement was applied along the top edge of the bearing

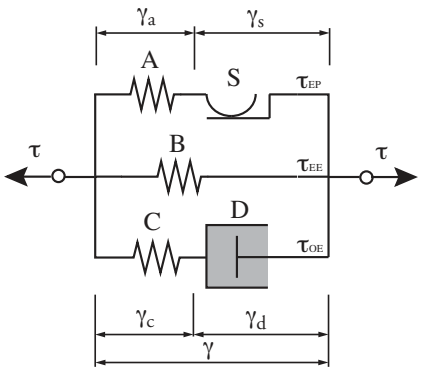

Fig.3 Rheology model. Superimposed shear stress response $\tau = \tau_{ep} + \tau_{ee} + \tau_{oe}$, where τ_{ep}, τ_{ee} and τ_{oe} represent the rate-independent elasto-plastic stress, nonlinear elastic stress, and the nonlinear viscoelastic overstress, respectively.

and the force response was measured by a number of load cells. All tests were carried out at around 23 °C. All specimens were preloaded by a sequence of 11 cycles of sinusoidal loading with 1.75 strain level and 0.05 Hz before conducting the actual loading tests. The preloading was done to remove the Mullins softening effect[14)] from the other inelastic behavior of the bearings. Further details of the test procedure are available in Bhuiyan et al[3)] and Bhuiyan[2)]. Tests on LRB and RB at low temperature (-20°C) were conducted by mounting the specimens within a closed chamber installed within the testing machine. Sufficient time was allowed to equilibrate the temperature within the specimen.

3. RHEOLOGY MODEL AND PARAMETER IDENTIFICATION SCHEME

Test results presented in **Fig. 1** illustrated the fundamental motivations for decomposing the stress and strain in the general rheology model, hereinafter referred to as the rheology model. **Fig. 3** presents the model and the schematic decomposition of stress and strain. The model comprises of three branches: the first branch implies the elasto-plastic behavior, the second one represents the nonlinear elastic behavior, and the third one describes the rate-dependent behavior of the bearings. The experimental scheme to characterize the nonlinear dependence of viscosity in loading/unloading phases follows from our earlier communication[3)]. The total shear stress response is decomposed into three branches acting in parallel:

$$\tau = \tau_{ep}(\gamma_a) + \tau_{ee}(\gamma) + \tau_{oe}(\gamma_c) \qquad (1)$$

where the shear stress is the total horizontal force at top of the bearings divided by the cross sectional area of the bearing. The shear strain is introduced by

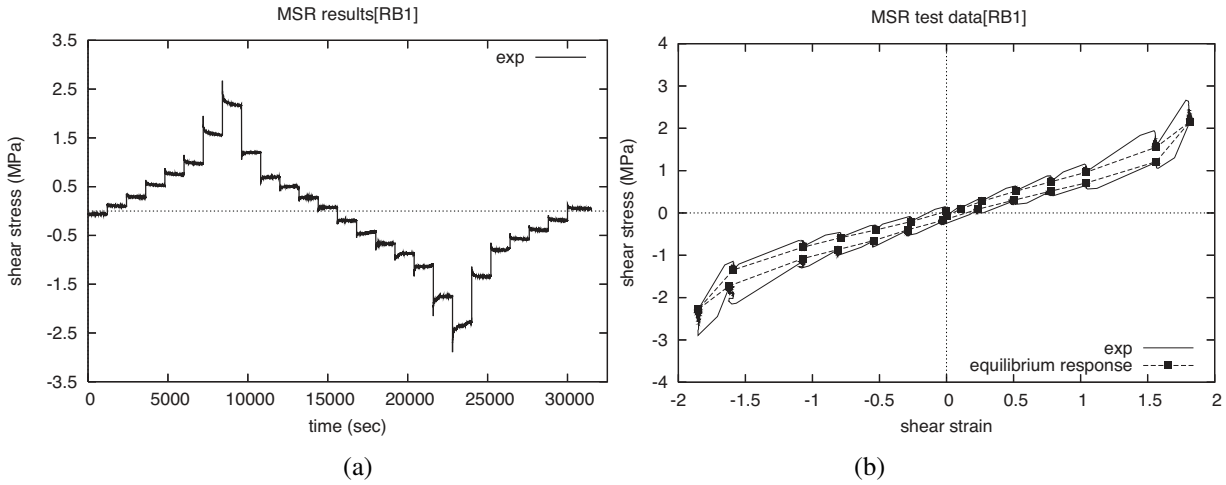

(a) (b)

Fig.4 MSR test results of RB (a) stress history (b) equilibrium stress response; equilibrium response at a particular strain level shows the response, which is asymptotically obtained from the shear stress histories. The experimental results obtained from the MSR test are presented by solid lines and points. The model results are indicated by the dashed lines.

two different decompositions into elastic and inelastic parts:

$$\gamma = \gamma_a + \gamma_s = \gamma_c + \gamma_d \tag{2}$$

where and are shear strain in spring A and C, respectively; the shear strain is the relative horizontal displacement between top and bottom edge of the bearing divided by the total thickness of the rubber layers. The first branch comprising of a spring (Element A) and a slider (Element S) represents the elasto-plastic response (τ_{ep}), the second branch containing a spring (Element B) represents the nonlinear elastic response (τ_{ee}), and these two branches together constitute the equilibrium response. On the other hand, a spring (Element C) along with the previous two branches represent the instantaneous response and the dashpot (Element D) represents the overstress (τ_{oe}) resulting from the rate-dependent effect.

4. IDENTIFICATION OF MODEL PARAMETERS FROM MEASUREMENTS

The parameters for rate-dependent and rate-independent branches of the model are derived from experiments and following the general characterization scheme presented in Bhuiyan *et al.*[3]. The equilibrium response is obtained by using MSR test data and the instantaneous response can be obtained for an infinitely fast loading rate[7),15),16)] through Cyclic Shear (CS) tests. The equilibrium and instantaneous responses thus obtained are regarded as the rate-independent elasto-plastic responses. The viscosity is characterized from Simple Relaxation (SR) tests at different maximum strain amplitudes. Subsection (1)–(3) are devoted towards introducing the original rheology model, while a simplified version is presented in Subsection (5).

(1) Equilibrium Response

Fig. 4 and **5** present the experimental results of RB and LRB obtained in MSR tests. **Fig. 4**(a) shows the resultant stress histories obtained from RB, in which the trend of convergence of the stress history to an almost constant stress value at the end of each relaxation period is clear. By connecting all the constant stress values obtained at respective strain levels, rate-independent stress responses are obtained (**Fig. 4**(b)). The time-independent stress responses are regarded as the equilibrium response at respective strain levels[16)]. The same phenomena were also observed in LRB specimen illustrated in **Fig. 5**(a) and **5**(b). In addition, the difference of the stress responses between loading and unloading gives the equilibrium hysteresis, which can be visualized in **Fig. 4**(b) and **5**(b) for RB and LRB, respectively. Furthermore, by comparing the stress histories obtained for RB and LRB (e.g. **Fig. 4**(b) and **5**(b)), it is observed that the decreasing trend in stress response of LRB is very fast in the first 20 min of each relaxation period. The contrast behavior is associated with the difference in viscosity properties of LRB and RB. The observations also fit well with the known constitutive properties of rubber as reported in different literatures[7),8),11),16)].

Moreover, a strain hardening feature at large strain levels is found to induce significant nonlinearities in the equilibrium hysteresis loop (**Fig. 4**(b) and **5**(b)). The equilibrium hysteresis can be reproduced by combining the nonlinear elastic response with the idealized elasto-plastic response[17)]. A spring-slider element is used to represent the elasto-plastic response

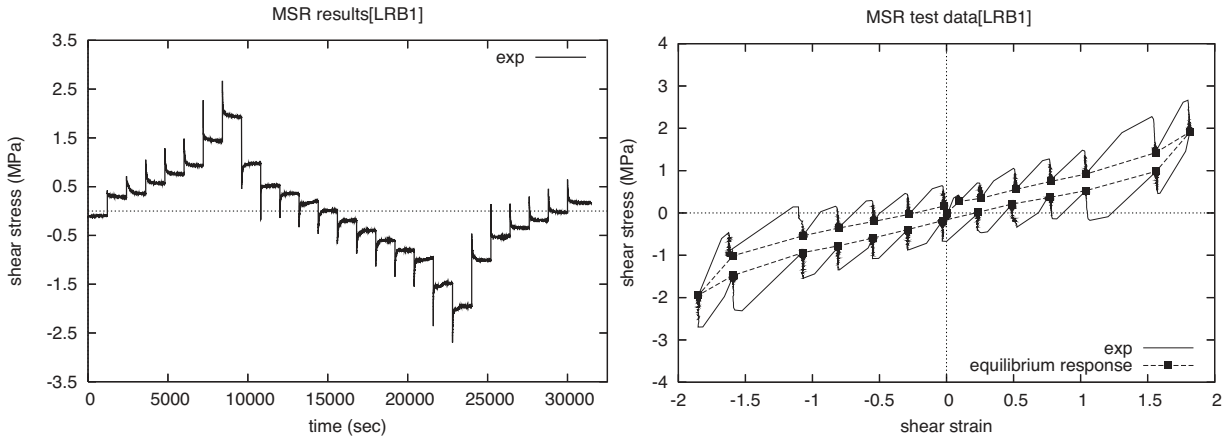

(a) (b)

Fig.5 MSR test results of LRB (a) stress history (b) equilibrium stress response; equilibrium response at a particular strain level shows the response, which is asymptotically obtained from the shear stress histories. The experimental results obtained from the MSR test are presented by solid lines and points. The model results are indicated by the dashed lines.

Table2 Parameters of the rheology model at +23 °C.

Type of bearings	C_1 MPa	C_2 MPa	C_3 MPa	C_4 MPa	τ_{cr} MPa	A MPa	m	n
RB	1.95	0.799	0.005	0.40	0.13	0.55	7.80	0.23
RB-2	2.05	0.883	0.006	0.40	0.11	0.43	7.23	0.24
LRB	4.25	0.710	0.003	1.35	0.19	0.73	8.24	0.27
LRB-2	4.18	0.779	0.010	1.35	0.23	0.79	6.68	0.30

of the bearing, which is placed at the top of the model (spring A and slider S). The shear stress-strain relation of the element A can be expressed as

$$\tau_{ep} = C_1 \gamma_a \tag{3}$$

where C_1 is a constant.

Element S is a friction slider. The friction slider will be active, when the stress level in the slider reaches a critical shear stress τ_{cr} i.e.

$$\begin{cases} \dot{\gamma}_s \neq 0, & |\tau_{ep}| = \tau_{cr}, \\ \dot{\gamma}_s = 0, & |\tau_{ep}| < \tau_{cr} \end{cases} \tag{4}$$

The critical shear stress τ_{cr} is estimated by using the equilibrium hysteresis loop (e.g. **Fig. 4**(b) and **5**(b)). The difference between the upper and the lower stress values in the equilibrium hysteresis loop at the same strain level corresponds to $2\tau_{cr}$, which in turn yields the critical shear stress for each bearing. The parameter C_1 is determined by fitting the initial part as well as switching parts from loading to unloading in the equilibrium hysteresis loop. The values of τ_{cr} and C_1 for each bearing are given **Table 2** for both sets of specimens.

The nonlinear elastic response of the bearing is represented by a non-Hookean spring (element B). The shear stress-strain relation of the element B can be defined as

$$\tau_{ee} = C_2 \gamma + C_3 |\gamma|^m sgn(\gamma) \tag{5}$$

where C_2, C_3, and m are constants and

$$sgn(x) = \begin{cases} +1, & x > 0, \\ 0, & x = 0, \\ -1, & x < 0 \end{cases} \tag{6}$$

The nonlinear elastic response shown in Eq.(5) can be determined by subtracting the stress response given by Eq. (3) from the equilibrium hysteresis obtained from the MSR test data. Nonlinear elasticity parameters C_2, C_3 and m are determined using a standard nonlinear least-square method. The values of these parameters are also given in **Table 2**. The equilibrium hysteresis computed using the proposed model and that obtained from the MSR test data are presented in **Fig. 6** to show the adequacy of Eq. (5) in reproducing the nonlinearity at large strains.

(2) Instantaneous response

Fig. 7 shows the rate-dependent shear stress-strain responses observed from the CS test data conducted at four different strain rates. A comparison of the stress responses at different strain rates of each bearing shows that with increasing the strain rates, the

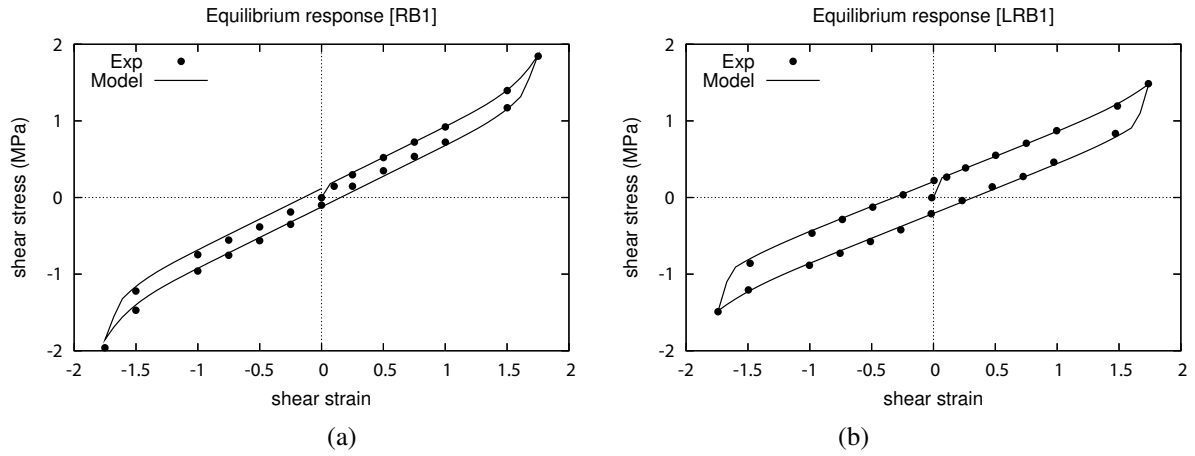

(a) (b)

Fig.6 Identification of equilibrium response parameters (a) RB and (b) LRB; the experimental results are obtained from MSR tests in asymptotic sense and the model results are determined using $\tau = \tau_{ep} + \tau_{ee} + \tau_{oe}$ with parameters given in **Table 2**.

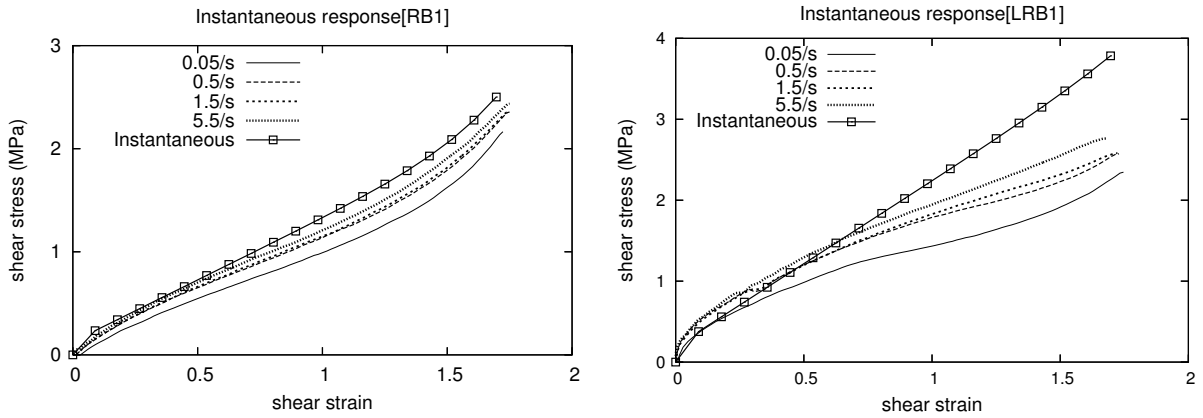

(a) (b)

Fig.7 Identification of instantaneous response parameters (a) RB and (b) LRB; the instantaneous response is determined using the model $\tau = \tau_{ep} + \tau_{ee} + \tau_{oe}$ (without dashpot element D) with parameters given **Table 2** and the experimental results represented by different lines are obtained from CS tests at four strain rates of 0.05, 0.5, 1.5, and 5.5 1/sec in loading regimes.

stress responses increase due to viscosity effect. At higher strain rates, however, a diminishing trend of the stress response was observed in both the bearings. This trend indicates the neighboring state of the instantaneous response of the bearings. In the current experimental scheme, the stress responses obtained at strain rates of 1.5/s and 5.5/s are regarded as the neighborhood of instantaneous responses of RB and LRB, respectively. At the instantaneous state, the structure of the rheology model can be reduced into the same model without the dashpot (Element D) (**Fig. 3**). This response can be obtained by adding the equilibrium stress and the stress in the third branch without the dashpot. The instantaneous response represented by spring C is nonlinear (**Fig. 7**). However, for simplicity, a linear spring model for spring C is considered:

$$\tau_{oe} = C_4 \gamma_c \tag{7}$$

where C_4 is a constant. The parameter C_4 is determined so that the instantaneous stress-strain curves obtained from the CS tests are enclosed by that computed using the rheology model (without the dashpot element) through trials. The obtained parameters C_4 for all bearings are listed in **Table 2** for both specimen sets.

(3) Characterization of nonlinear viscosity

Fig. 4 and **5** presented the viscosity induced stress relaxation feature in RB and LRB observed via MSR tests. To eliminate the possible influence of past strain history on the viscosity effect, SR tests were conducted for different strain levels. **Fig. 8** presents the

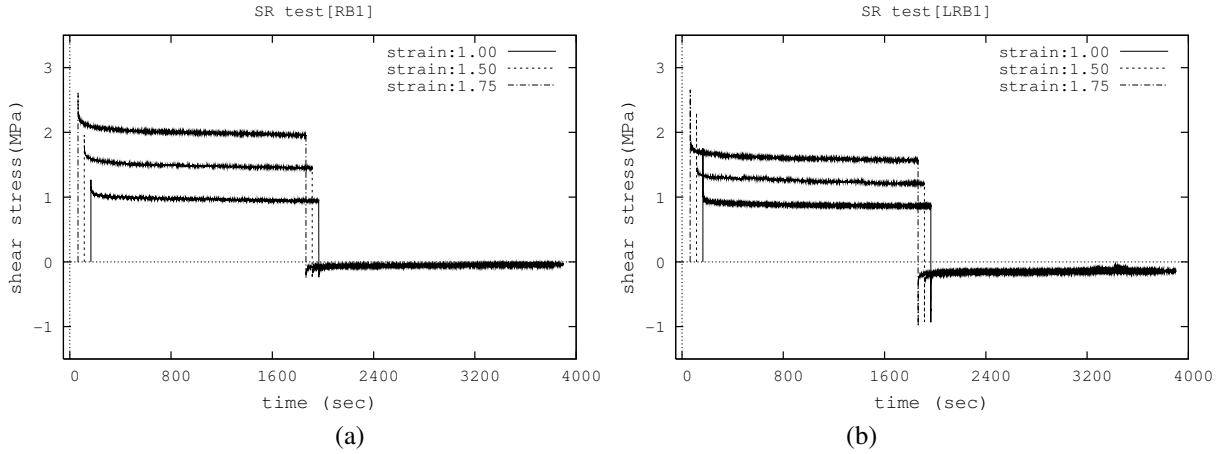

(a) (b)

Fig.8 Stress histories obtained from SR tests at different strain levels (a) RB (b) LRB. For clear illustration, the stress histories have been separated by 50 sec to each other.

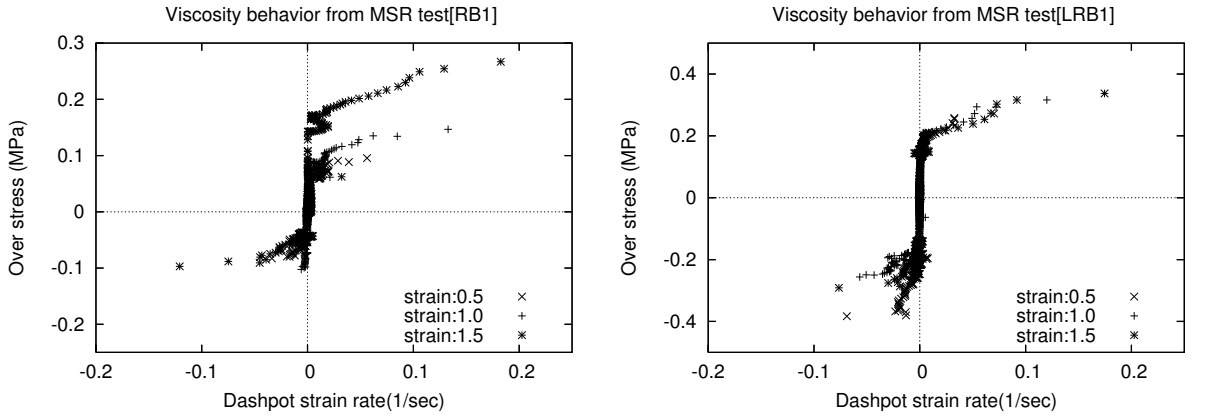

(a) (b)

Fig.9 Overstress-dashpot strain rate relations obtained from MSR tests at different strain levels in loading and unloading regimes (a) RB and (b) LRB; the values in the legend stand for the total strains in respective relaxation processes after loading and unloading.

stress histories obtained from the SR tests. In both bearings (RB and LRB), a rapid stress relaxation was displayed at all strain levels in the first few minutes after while it approached asymptotically towards the equilibrium state. The amount of stress relaxation in loading/unloading of LRB was found to be higher than that of RB. The relatively high stress relaxation in LRB has the direct conformity with test results of the CS tests (e.g. **Fig. 7**).

In order to construct relation for the viscosity induced overstress (Element D) τ_{oe} and dashpot strain-rate $\dot{\gamma}_d$, the experimental data of SR and the MSR tests of the bearings are considered. The experimental results of MSR and SR tests are analyzed using the same methodology explained in the earlier communication[3]. **Fig. 9** shows the τ_{oe}–$\dot{\gamma}_d$ relations obtained using the MSR test data and the same obtained from SR data are presented in **Fig. 10**. The positive overstress indicates relaxation after loading and the negative values indicate relaxation after unloading. The observations presented in **Fig. 9** and **10** suggest the nonlinear dependence of the overstress upon the dashpot strain rates.

The existence of the viscosity effect in the loading and unloading phases of both LRB and RB is perceptible in **Fig. 8** to **10**. The effect was more significant in LRB than in RB, but not as prominent as appeared in HDRB[3]. Furthermore, the gradient of the τ_{oe}–$\dot{\gamma}_d$ curve denoting the viscosity of the device is found to depend on strain levels of the relaxation experiments in RB during loading; however in unloading, such an effect is not much visible (see, e.g. **Fig. 9**(a) and **10**(a)). In LRB, however, the gradient is not perceived to be related with the strain levels of the relax-

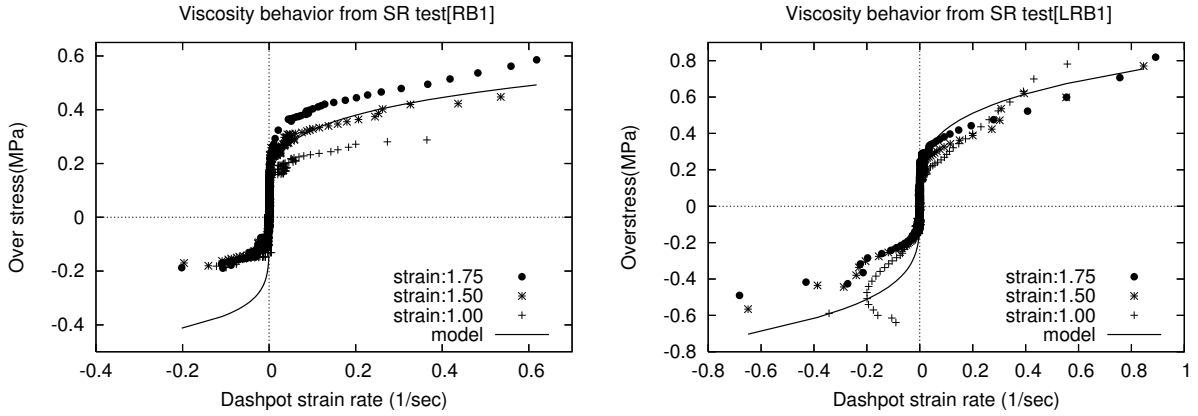

(a) (b)

Fig.10 Identification of viscosity parameters using SR test data (a) RB, (b) LRB; the model results represented by solid lines with parameters in **Table 2** and the τ_{oe}–$\dot{\gamma}_d$ relations calculated from SR test data are shown by points. The values in the legend stand for the total strains in respective relaxation processes, and 1.0, 1.5, 1.75 correspond to relaxation processes after loading, and 0 after unloading.

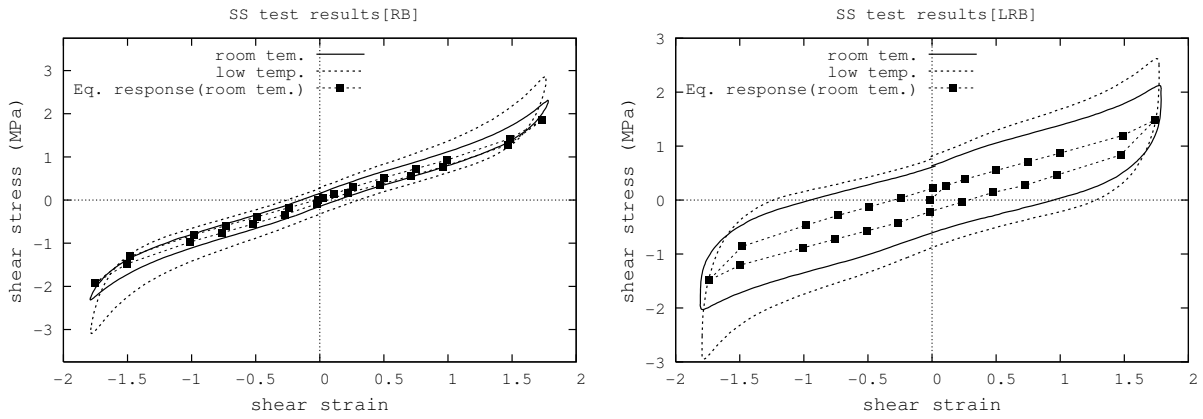

(a) (b)

Fig.11 Effect of temperature in stress–strain responses of the bearing under sinusoidal loading (a) RB (b) LRB.

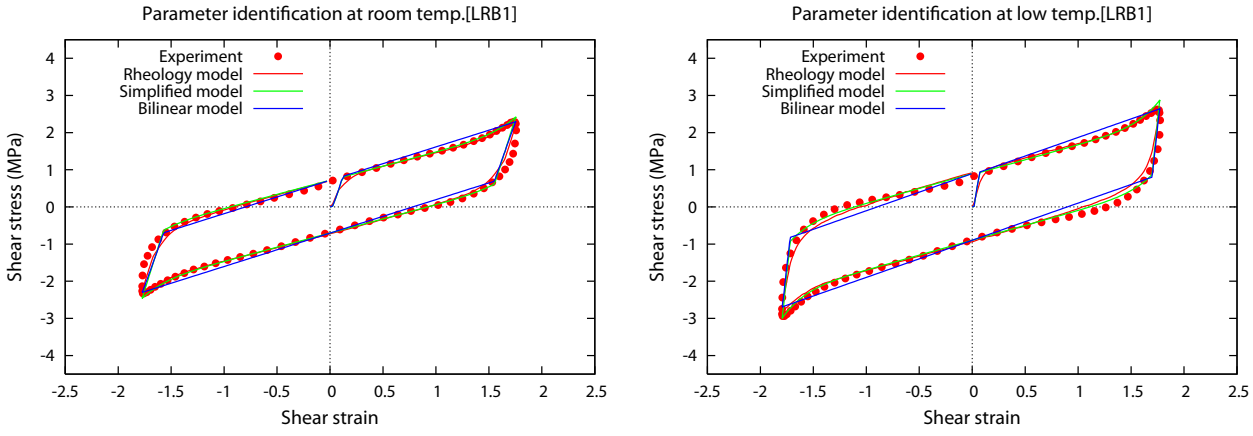

(a) (b)

Fig.12 Numerical simulation of sinusoidal excitation of LRB at (a) room temperature (+23°C), and (b) low temperature (−20°C).

ation experiments (e.g. **Fig. 9**(b), **Fig. 10**(b)). As opposed to HDRB[3] that displayed a strong dependence of viscosity induced overstress effect on the current strain level in both loading and unloading, the exper-

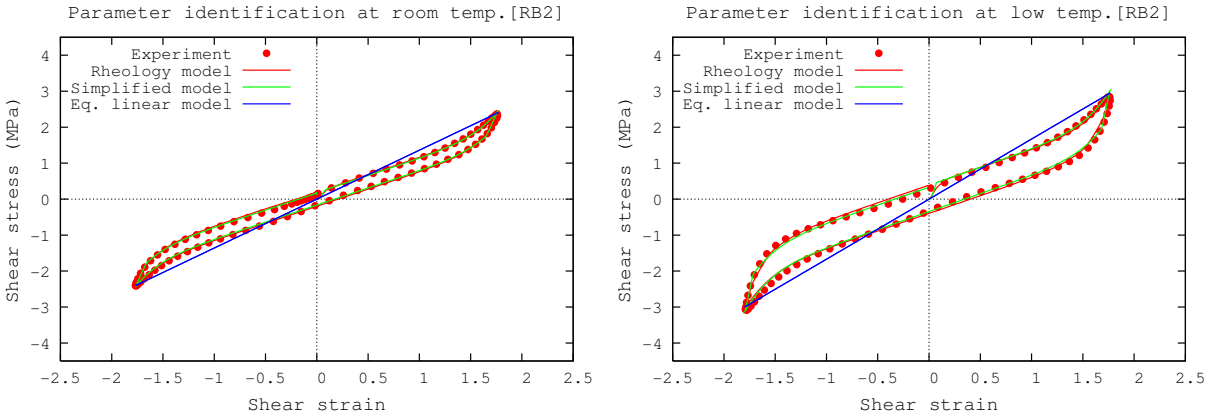

(a) (b)

Fig.13 Numerical simulation of sinusoidal excitation of RB at (a) room temperature (+23 °C), and (b) low temperature (−20°C).

Table3 Viscosity parameters for LRB and RB at +23 °C determined for simulation of sinusoidal loading tests.

Specimen	A (MPa)	n
RB	0.050	0.23
LRB	0.300	0.27

imental evidences presented in this paper on RB and LRB suggest weak dependency. In addition, τ_{oe}–$\dot{\gamma}_d$ relation in RB and LRB in loading seems to be analogous to that in unloading, whereas in HDRB it was vividly different. Motivated by the characteristic τ_{oe}–$\dot{\gamma}_d$ relationships obtained from the MSR and the SR tests of RB and LRB shown in **Fig. 9** and **10**, the relation to represent the dashpot (Element D) is proposed to be expressed by

$$\tau_{oe} = A \left| \frac{\dot{\gamma}_d}{\dot{\gamma}_0} \right|^n sgn(\dot{\gamma}_d) \tag{8}$$

where $\dot{\gamma}_0 = 1.0$ sec^{-1} is a reference strain rate of the dashpot, A and n are the nonlinear viscosity parameters. τ_{oe}–$\dot{\gamma}_d$ relationships obtained from the SR test data correspond to Eq. (8). Using a standard numerical method, the parameters are determined. The overstress-dashpot strain rate curves of RB and LRB obtained from SR tests and the proposed model are presented in **Fig. 10**(a) and **10**(b), respectively. The identified parameters of the model are given in **Table 3**.

(4) Sinusoidal loading tests and the effect of temperature

The effect of ambient temperature on the response of the bearings is illustrated in **Fig. 11** to **13**. In these tests, the specimens were subjected to an 11 cycle sinusoidal loading with 1.75 shear strain amplitude and 0.5 Hz frequency. Tests were conducted for two difference room temperatures, e.g. +23 °C and −20°C. All specimens were kept in a temperature control testing room more than 12 hours before a test to obtain the same initial temperature of specimens as the room temperatures. In order to remove the Mullins effect[14] of bearings, the 4th cycle shear stress-strain responses are considered and plotted. The viscosity parameters of the models to be used in seismic analysis of the bridge (Section 5) are also determined from these test results. By comparing the results, it is evident that hysteresis effect is larger in both RB and LRB at low temperature. Furthermore, a distinct increase in the nonlinearity of the stress-strain response marked by strain hardening feature at large strain is clear. The viscosity parameters re-evaluated from sinusoidal tests at +23 °C and used for simulation are presented in **Table 3**. The elasticity and viscosity parameters determined from sinusoidal tests at −20°C are given in **Table 4**.

(5) Simplified model with hardening

A comparison of the stress-strain responses obtained from sinusoidal tests at room temperature (+23 °C) and at low temperature (−20°C) revealed the dominance of nonlinearity in the response. The feature is more prominent at low temperature (Subsection 4(4)). Furthermore, Subsections 4(1)–(3) have shown the existence of weak rate-dependency in LRB and more particularly in RB. All these observations suggest the promise of further simplification of the general rheology model (Subsections 4(1)–(3)). Essentially, such simplification can be feasible by preserving the nonlinear elastoplastic branches of the rheology model (**Fig. 3**). **Fig. 14** presents a proposal for the simplified structure of the rheology model. In this model, the total shear stress is decomposed into

Table4 Elasticity and viscosity parameters of the rheology model at -20°C.

Type of bearings	C_1 MPa	C_2 MPa	C_3 MPa	C_4 MPa	τ_{cr} MPa	A MPa	m	n
LRB	6.521	0.830	0.004	5.521	0.190	0.391	8.941	0.272
RB	3.800	0.980	0.015	1.700	0.110	0.200	7.134	0.140

Table5 Parameters of the simplified model for simulation of sinusoidal loading tests.

	C_1 (MPa)		C_2 (MPa)		C_3 (MPa)		τ_{cr} (MPa)		m	
	+23°C	−20°C	+23°C	−20°C	+23°C	−20°C	+23°C	−20°C	+23°C	−20°C
LRB	7.500	27.52	0.760	0.800	0.004	0.004	0.680	0.795	8.070	8.741
RB	3.501	9.800	0.950	1.000	0.008	0.015	0.160	0.310	7.534	7.134

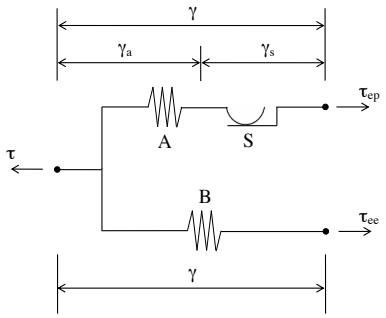

Fig.14 Decomposition of stress and strain in the simplified model.

Table6 Parameters of the design model for LRB.

	C_1 (MPa)	C_2 (MPa)	τ_{cr} (MPa)
23 °C	7.500	0.900	0.680
−20°C	27.52	1.000	0.795

two contributions associated with a nonlinear elastic stress and an elasto-plastic stress, and hence the third branch (τ_{oe}) of the rheology model is discarded. In this case, five parameters are required to represent the stress-strain responses of the bearings: C_1 parameter corresponds to the initial shear modulus; C_2 the post yield shear modulus; τ_{cr} the yield strength, and the parameters C_3 and m are used to represent the strain hardening property of the bearing at high strain levels. The model parameters determined from the sinusoidal loading tests are presented in **Table 5** for two temperature conditions.

(6) Design models

Finally, the conventional design models[4),5)] are revisited here for evaluating the parameters and use in the simulation comparisons presented in this section.

Table7 Geometric and material properties of the piers (unit: mm).

Particulars	Pier S1, S2	Pier P1 to P4
Pier cap B1 × W1	3300 × 9600	2000 × 9600
Pier body B2 × W2	3300 × 6000	2000 × 6000
Footing B3 × W3	5000 × 8000	5000 × 8000
No. of piles/pier	4	4

a) Bilinear model

The bilinear model of the bearings can be recovered after simplification of the proposed rheology model (Subsection 4(1)–(3)). The simplified structure of the model is formed by using a linear elastic response (τ_{ee}) and an elasto-plastic response (τ_{op}) only and hence the third branch (τ_{oe}) of the model is discarded. In this case, three parameters are required to represent the bilinear relationships of stress-strain responses of the bearings: C_1 parameter corresponds to the initial shear modulus, C_2 the post yield shear modulus, and τ_{cr} the yield strength of the bearings. Eq. (9) presents the bilinear model.

$$\tau_{ep} = C_1\gamma_a \ \text{ with } \begin{cases} \dot{\gamma}_s \neq 0, & |\tau_{ep}| = \tau_{cr}, \\ \dot{\gamma}_s = 0, & |\tau_{ep}| < \tau_{cr} \end{cases} \tag{9}$$

$$\tau_{ee} = C_2\gamma \tag{10}$$

where C_1, C_2, τ_{cr} are the parameters determined from sinusoidal experiments (**Fig. 4**) and listed in **Table 6**.

b) Equivalent linear model

An equivalent linear model is employed for RB in the numerical analysis. Two parameters are required for this model: the equivalent stiffness and damping constant. The equivalent stiffness of the bearing can be evaluated using the nominal shear modulus G_e of the rubber material (1.2 MPa, **Table 1**). The damping constant of the bearing is usually assumed to in the range of 0.03 to 0.05.

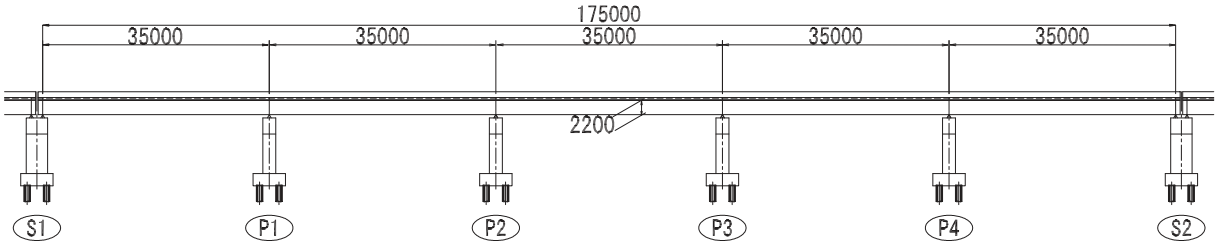

(a) Side view

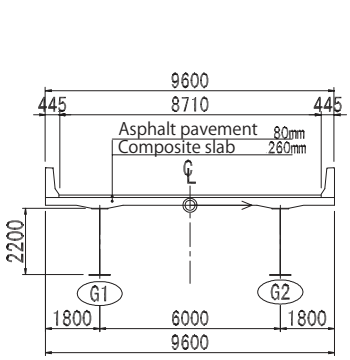

(b) Cross section of superstructure

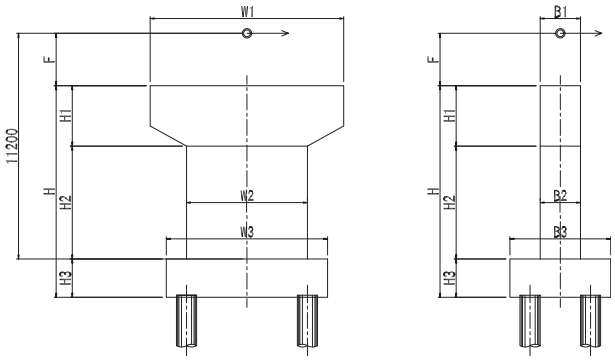

(c) Concrete bridge pier

Fig.15 Model bridge for seismic analysis; all dimensions are in mm. In the figure, H1 = 3000mm, H2 = 5600mm, H3 = 2000mm, F = 2200mm. [2)]

5. PROTOTYPE BRIDGE FOR SEISMIC ANALYSIS

Table 2 to **6** provide parameters for three different models of the bearings at two different ambient temperatures. Among these models, nonlinearity in the stress-strain response is taken into account in both the general rheology model (Subsections 4(1)-(3)) and the simplified model (Subsection 4(5)), while the rate-dependency effect is considered only in the general rheology model. On the other hand, the design models (Subsection 4(6)) consider none of these effects. Therefore, it is motivating to investigate the effectiveness of all these different versions of the models for LRB and RB in simulating the design parameters by comparing results from a benchmark design problem. In this connection, the analytical model of the prototype bridge S-P-F system shown in **Fig. 15** is considered. The substructures consist of RC piers and footings supported on pile foundations. The geometry and material properties of the bridge deck, piers with footings are given in **Fig. 15** and **Table 7**. **Table 8** presents the geometry of the HDRB. All dimensions of the model bridge are determined by trial design with a bilinear model for rubber bearing hysteresis model in accordance with a design specifications[4)].

The analytical model of the bridge S-P-F system is shown in **Fig. 16**. The entire structural system is approximated as a 2-D frame. A finite element model with frame and spring elements is used to model the bridge system. The superstructure of the bridge is modeled with elastic beam elements. The concrete piers are modeled elastic beam elements with a plastic hinge. Takeda tri-linear model[18)] is used to model the hysteretic behavior of the plastic hinge in each pier. In the analysis, two linear springs are used for taking into account the ground-foundation interaction: translational and rotational springs; see the dissertation[2)] for more details of modeling.

Table8 Geometric dimensions of HDRB in prototype bridge

Particulars	Specifications
Cross-section (mm^2)	650×650
Number of rubber layers	6
Thickness of one rubber layer (mm)	13.54
Thickness of steel layer (mm)	2.3
Nominal shear Modulus (MPa)	1.2

The following section will be devoted to reporting the simulation results, comparisons and critical discussions.

6. SEISMIC RESPONSES OF BRIDGE

Fig. 17 and **18** present typical shear stress-strain responses of the bearings installed at top of a pier of the prototype bridge (**Fig. 2**) subjected to Level 2

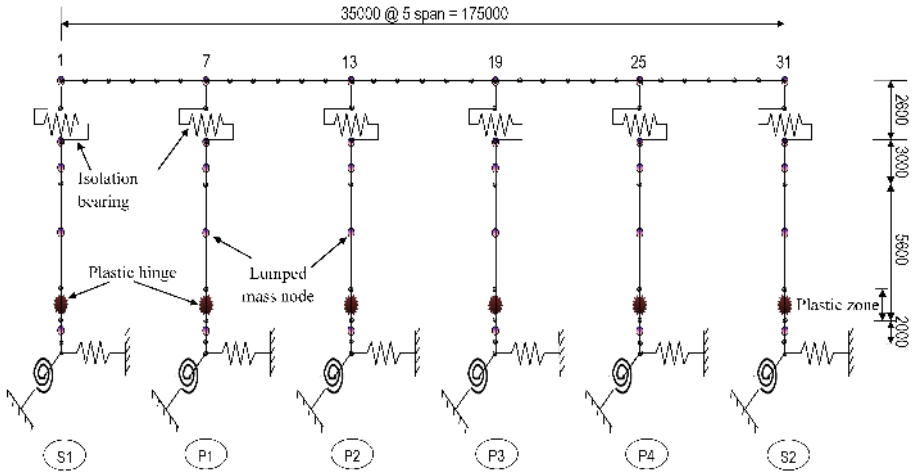

Fig.16 Analytical model of bridge.

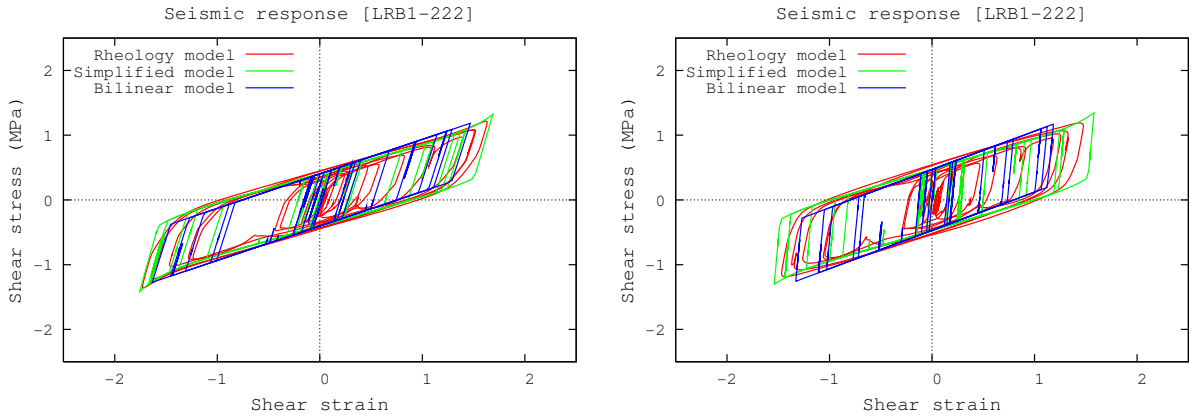

(a) (b)

Fig.17 Shear stress-strain responses of the isolation bearings LRB at the top of the P1 (=P4) piers as obtained for Level 2 Type II earthquake ground motion at (a) room temperature (+23°C) and (b) low temperature (−20°C).

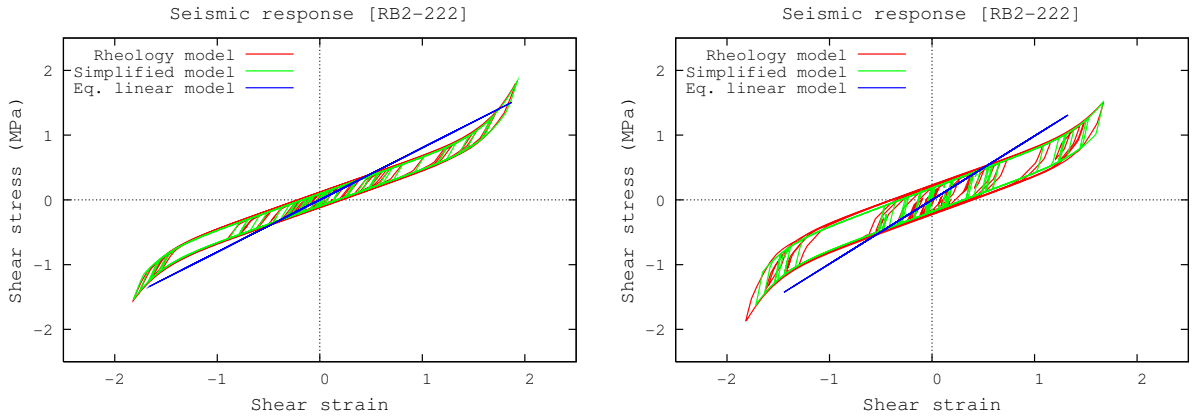

(a) (b)

Fig.18 Shear stress–strain responses of the isolation bearings RB at the top of the P1 (=P4) piers as obtained for Level 2 Type II earthquake ground motion at (a) room temperature (+23°C) and (b) low temperature (−20°C).

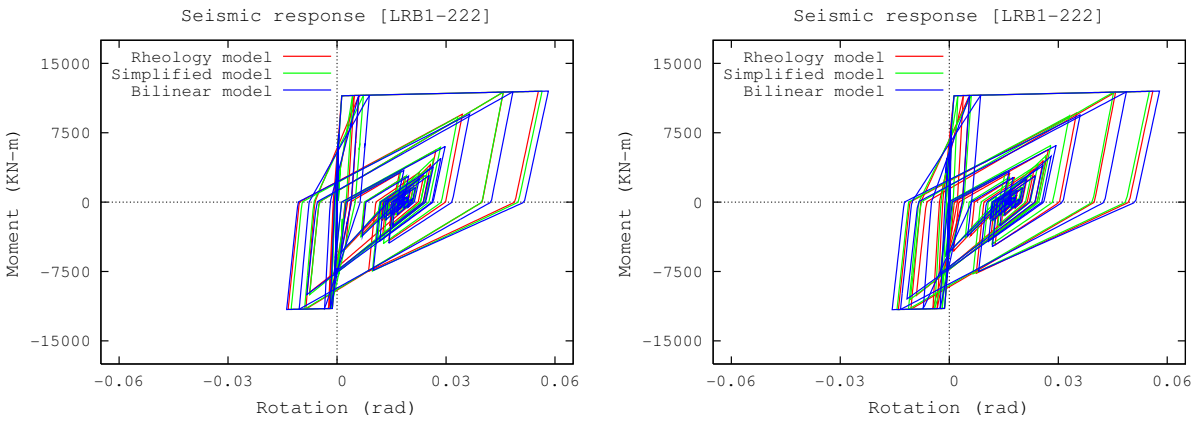

Fig.19 Moment-rotation responses of plastic hinge of the pier P1 (=P4) as obtained using LRB bearings for Level 2 Type II earthquake ground motion at (a) room temperature (+23 °C) and (b) low temperature (−20°C).

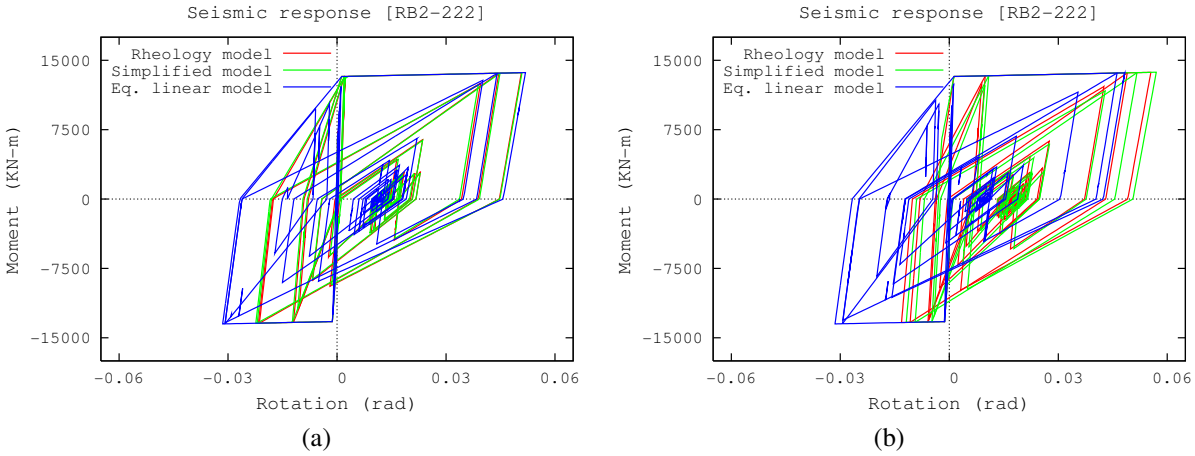

Fig.20 Moment-rotation responses of plastic hinge of the pier P1 (=P4) as obtained using RB bearings for Level 2 Type II earthquake ground motion at (a) room temperature (+23 °C) and (b) low temperature (−20°C).

earthquake (severe) ground motions[4]. **Fig. 19** and **20** present the plot of moment-rotation responses for the plastic hinge modeled by the Takeda tri-linear model. The plots are related only to P1(=P4) pier and Type II earthquake but for two temperature conditions. The other results are skipped here for space limitation. From these results, it is evident that the bearing responses are in close agreement for both the rheology model and the simplified model. The function of the Takeda tri-linear model in simulating the model rotation responses after formation of plastic hinge at the bottom of the pier is distinctly visible.

As shown in **Fig. 17**(b), the maximum shear strain in LRB at low temperature estimated by the design model was seen about 30% less than the rheology and simplified model. However, in room temperature (**Fig. 17**(a)) the difference of the maximum shear strain in the design and simplified models is not significant. Similar trend of the results can be observed from **Fig. 18**(a) and (b) in case of RB. In low temperature, the design model estimated about 25% less shear strain than the simplified model in the case of RB.

Moreover, as shown in **Fig. 20**(b), the maximum rotation of the bridge pier isolated by RB at low temperature estimated by the design model was seen about 23% less than the rheology and simplified model. However, in room temperature (**Fig. 20**(a)) the difference of the maximum rotation in the design and simplified models is not significant. In case of LRB as shown in **Fig. 19**(a) and (b), the difference in rotation by the design and simplified models is not considerable.

Finally, in order to obtain a comprehensive assessment of the bearing models in the response prediction of the bridge S-P-F system, some key parameters for bridge design, namely, the shear strain of the bearing and rotation of the pier are plotted in **Fig. 21** to

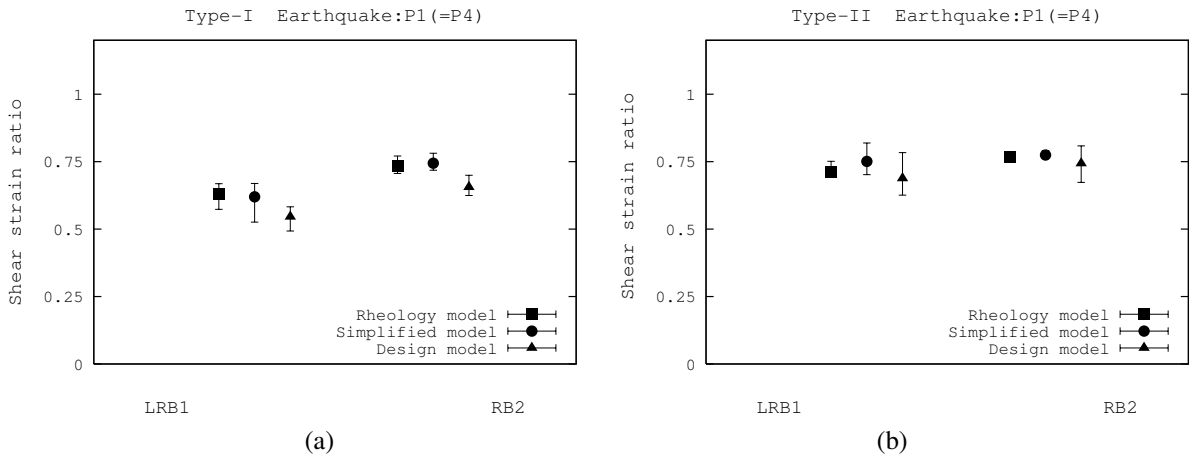

Fig.21 Comparison of maximum shear strain ratios occurred at top of the isolation bearings at +23°C due to Level 2, (a) Type I (b) Type II, earthquake ground motion. Shear strain ratio is the maximum shear strain of the isolation bearings divided by the allowable shear strain.

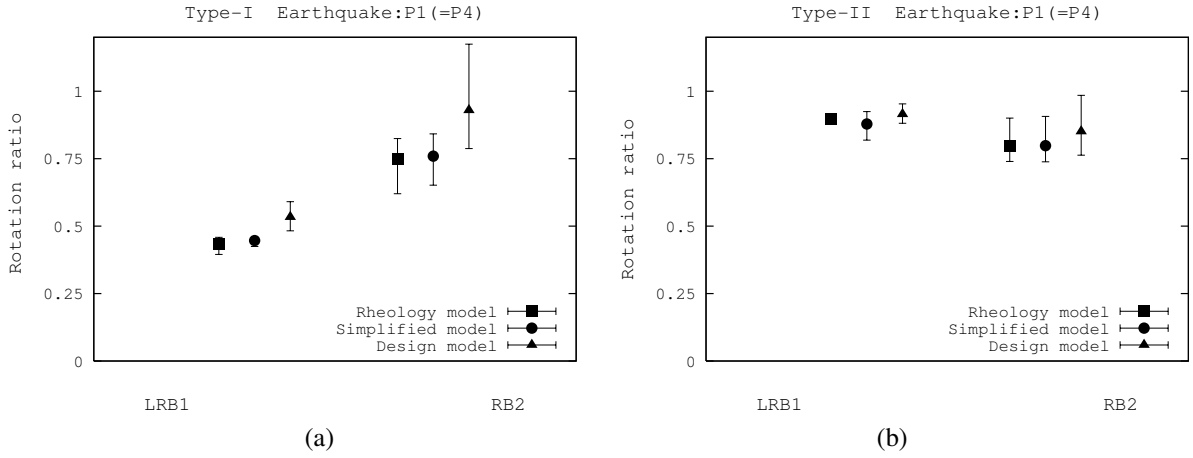

Fig.22 Comparison of maximum rotations of pier P1 (=P4) at +23°C due to Level 2, (a) Type I (b) Type II earthquake ground motion for different isolation bearings; Rotation ratio is the maximum rotation of the pier at the plastic hinge level divided by the allowable rotation.

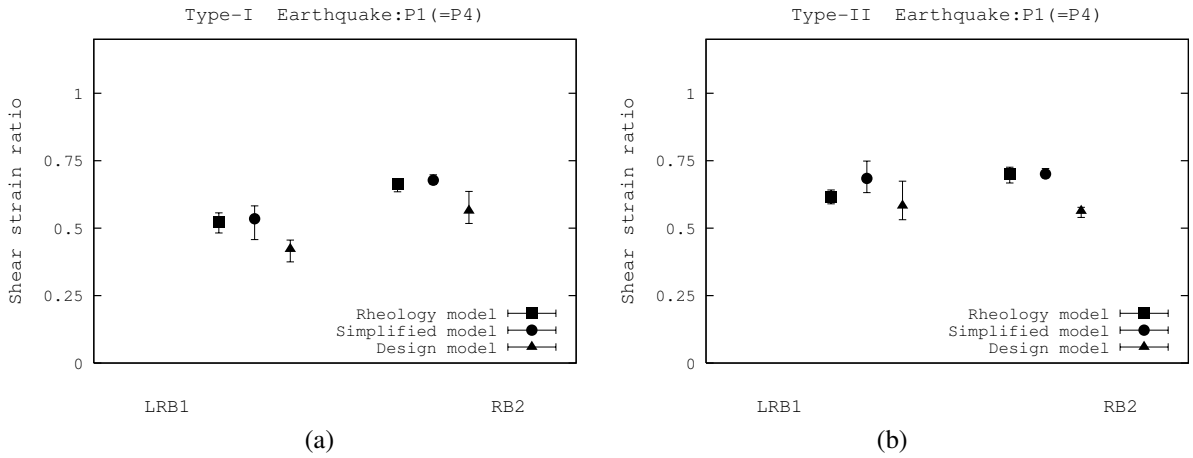

Fig.23 Comparison of maximum shear strain ratios of the isolation bearings at −20°C due to Level 2, (a) Type I (b) Type II, earthquake ground motion. Shear strain ratio is the maximum shear strain of the isolation bearings divided by the allowable shear strain.

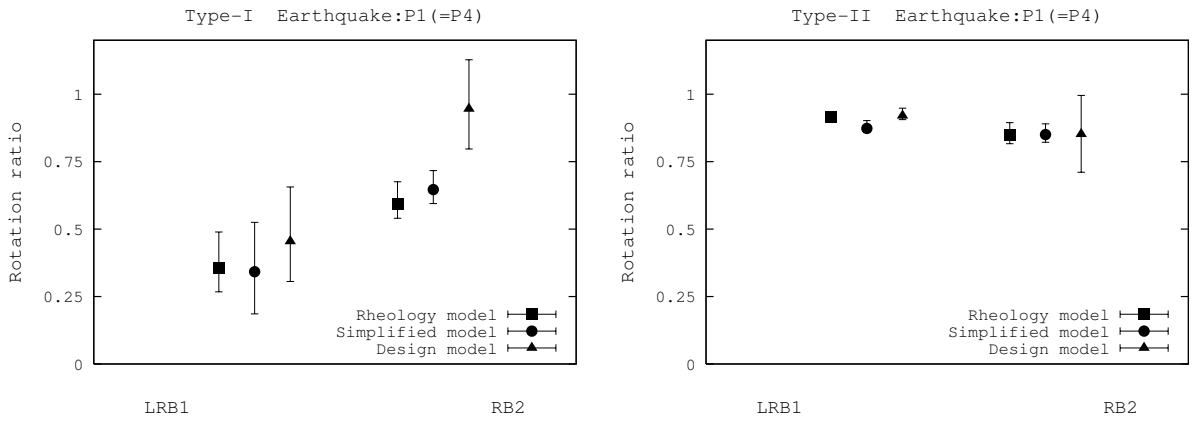

Fig.24 Comparison of maximum rotations of pier P1 (=P4) at -20°C due to Level 2, (a) Type I (b) Type II earthquake ground motion for different isolation bearings; Rotation ratio is the maximum rotation of the pier at the plastic hinge divided by the allowable rotation.

24 for two temperatures and two earthquake ground motions, each having three records. In plotting the results, the maximum, minimum and the arithmetic mean of the bridge design parameters are presented. From these figures, the responses obtained from the simplified model for both rubber bering and pier are almost identical with those obtained from the rheology model. For both temperatures, the rotation response of piers obtained from the design model are substantially different from the simplified model. In particular, the difference becomes prominent at low temperature; and the differences at +23°C and -20°C are about 15 and 28%, respectively. At -20°C, the rubber bearing responses obtained from the design model are about 10% smaller than those from the simplified model.

7. CONCLUDING REMARKS

A general and a simplified version of rheology model are presented in this paper to represent the rate-dependent elasto-plastic behavior of RB and LRB. The effect of modeling for bearings in the proposed approach on the seismic responses of the isolated bridge is evaluated by conducting nonlinear dynamic analyses. The model parameters used in the simulation have been identified from experimental measurements under room and low temperature conditions. Three different analytical models of the isolation bearings (LRB and RB); namely the design model[4], the general rheology model and the simplified model are considered in simulation. The performance of the models is discussed in terms of the moment-rotation relations of the plastic hinges and the shear stress-strain relations of the bearings, since these responses are very crucial for seismic design of bridge systems. The results indicate that a careful selection of the models of isolation bearings is important for seismic design of an isolated bridge S-P-F system, especially for low temperatures. In addition, a systematic methodology to identify the rheology model parameters for isolation bearings based on explicit experimental evidence is presented. We have addressed the significant aspects that are necessary to consider in composing a benchmark S-P-F system in verifying the effectiveness of the bearing models in response prediction. Furthermore, a basis is presented for the design desk in comparing the relevant design parameters obtained using different models. The general applicability of the proposed methodology has been confirmed by applying the same on HDRB, LRB and RB specimens.

ACKNOWLEDGMENT: The experimental works were conducted by utilizing the laboratory facilities and bearings-specimens provided by Japan Rubber Bearing Association. The authors indeed gratefully acknowledge the kind cooperation extended by them. The authors also offer special thanks to Hokubu Consultant Ltd. and Seismic Engineering Inc. for providing necessary cooperation throughout this work. Furthermore, the authors sincerely acknowledge the funding provided by the Japanese Ministry of Education, Science, Sports and Culture (MEXT), and in the form of scholarships. This work was supported by JSPS KAKENHI Grant Number 22560473.

REFERENCES

1) Robinson, W.H.: Lead rubber hysteresis bearings for protecting structures during earthquakes, *Earthquake Engineering and Structural Dynamics*, Vol.10 pp.593-604, 1982.

2) Bhuiyan, A.R.: Rheology modeling of laminated rubber bearings, PhD Dissertation, Graduate School of Science and Engineering, Saitama University, 2009.
3) Bhuiyan, A.R., Okui, Y., Mitamura, H. and Imai, T.: A rheology model of high damping rubber bearings for seismic analysis: Identification of nonlinear viscosity, *International Journal of Solids and Structures*, Vol.46, pp.1778-1792, 2009.
4) Japan Road Association: Design Specification for Highway Bridges Part V: Seismic Design, 2002.
5) American Association of State Highways and Transportation Officials (AASHTO): Guide specification for seismic isolation design, 2/e, 2000.
6) Skinner, R.I., Robinson, W.H. and McVerry, G.H.: An introduction to seismic isolation, DSIR Physical Science, Wellington, New Zealand, 1993.
7) Amin, A.F.M.S., Alam, M.S. and Okui Y.: An improved hyperelasticity relation in modeling viscoelasticity response of natural and high damping rubbers in compression: experiments, parameter identification and numerical verification, *Mechanics of Materials*, Vol.34, pp.75-95, 2002.
8) Amin, A.F.M.S., Lion, A., Sekita, S. and Okui, Y.: Nonlinear dependence of viscosity in modeling the rate-dependent response of natural and high damping rubbers in compression and shear: Experimental identification and numerical verification, *International Journal of Plasticity*, Vol.22, pp.1610-1657, 2006.
9) Yakut, A. and Yura, A.J.: Evaluation of elastomeric bearing performance at low temperatures, *Journal of Structural Engineering*, ASCE, Vol. 128, No.4, pp. 995-1002, 2002.
10) Yakut, A. and Yura, A.J.: Parameters influencing performances of elastomeric bearings at low temperatures, *Journal of Structural Engineering*, ASCE, Vol.128, No.4, pp.986-994, 2002.
11) Amin, A.F.M.S., Lion, A. and Häfer, P.: Effect of temperature history on the mechanical behavior of a filler-reinforced NR/BR blend: literature review and critical experiments, *Journal of Applied Mathematics and Mechanics*, Vol.90, No.5, pp.347-369, 2010.
12) International Organization of Standardization (ISO): Elastomeric seismic-protection isolators, Part 1: Test methods, 2005.
13) Kelly, J.M.: *Earthquake Resistant Design with Rubber*, Springer-Verlag Berlin Heidelberg, New York, 1997.
14) Mullins, L.: Softening of rubber by deformation, *Rubber Chemistry and Technology*, Vol.42, pp.339-362, 1969.
15) Bergstrom, J.S. and Boyce, M.C.: Constitutive modeling of the large strain time-dependent behavior of elastomers, *Journal of Mechanics and Physics of Solids*, Vol.46, pp.931-954, 1998.
16) Lion, A.: A constitutive model for carbon black filled rubber: Experimental investigations and mathematical representation, *Continuum Mechanics and Thermodynamics*, Vol.8, pp.153-169, 1996.
17) Simo, J.C. and Hughes, T.J.R.: *Computational Inelasticity*, Springer-Verlag, New York, 1998.
18) Takeda, T., Sozen, M.A. and Nielsen, N.N.: Reinforced concrete response to simulated earthquakes, *Journal of the Structural Division*, ASCE, Vol.96, pp.2557-2573, 1970.

(Received August 22, 2011)